Supplementary Information:

Ferroelectric Modulation of Surface Electronic States in $BaTiO_3$ for Enhanced Hydrogen Evolution Activity

Pedram Abbasi[1], Matthew R. Barone[2], Ma. de la Paz Cruz-Jáuregui[3], Duilio Valdespino-Padilla[3,4], Hanjong Paik[5], Taewoo Kim[6], Lior Kornblum[7,8], Darrell G. Schlom[2,9,10], Tod A. Pascal[1], David P. Fenning[1,6]**

[1] Department of NanoEngineering, University of California San Diego, La Jolla, CA 92093, USA

[2] Department of Materials Science and Engineering, Cornell University, Ithaca, New York 14853, USA

[3] Centro de Nanociencias y Nanotecnología (CNyN)-Universidad Nacional Autónoma de México (UNAM) Km 107, Carretera Tijuana-Ensenada Ensenada B.C., C.P 22800, Mexico

[4] Universidad Autónoma de Baja California (UABC), Km 107, Carretera Tijuana-Ensenada Ensenada B.C., C.P 22800, Mexico

[5] Platform for the Accelerated Realization, Analysis & Discovery of Interface Materials (PARADIM), Cornell University, Ithaca, New York 14853, USA

[6] Chemical Engineering Program, Department of NanoEngineering, University of California San Diego, La Jolla, CA 92093, USA

[7]Andrew & Erna Viterbi Department of Electrical & Computer Engineering, Technion - Israel Institute of Technology, Haifa 32000-03, Israel

[8]The Nancy & Stephen Grand Technion Energy Program, Technion − Israel Institute of Technology, Haifa 32000-03, Israel

[9] Kavli Institute at Cornell for Nanoscale Science, Ithaca, New York 14853, USA

[10] Leibniz-Institut für Kristallzüchtung, Max-Born-Str. 2, 12489 Berlin, Germany

Corresponding authors: tpascal@ucsd.edu (T.A.P), dfenning@eng.ucsd.edu (D.P.F).

Keywords: *Ferroelectrics, Electrocatalysis, Spectroscopy, Density functional theory*

Extended Methods:

Material Synthesis:

The $BaTiO_3$ thin films (~15 nm thick) were deposited on (0.5 wt.%) Nb-doped (001)-oriented $SrTiO_3$ substrates ($Nb:SrTiO_3$) by reactive MBE in a Veeco GEN10 chamber. Prior to growth, the $Nb:SrTiO_3$ substrates were terminated following the procedure developed by Koster *et al.*[1] Elemental barium and titanium were supplied by a conventional effusion cell and a Ti-Ball,[2] respectively. During growth the background pressure was 5×10^{-7} Torr of (O_2 + 10% O_3) and the substrate temperature was 850˚C. Before growth of the $BaTiO_3$ on $Nb:SrTiO_3$, the fluxes of barium and titanium were calibrated by monitoring the RHEED intensity along the [110] azimuth during shuttered deposition of $BaTiO_3$ on a $GdScO_3$ (110) substrate, akin to the method previously developed for $SrTiO_3$.[3] Once the fluxes of barium and titanium were determined, the $BaTiO_3$ film was grown on $Nb:SrTiO_3$ by alternately supplying monolayer doses of BaO and TiO_2.

X-Ray Diffraction:

XRD measurements were performed by a Malvern Panalytical Empyrean Diffractometer using Cu K_α x-rays slitted to 0.5˚. When measuring the θ-2θ scan, scattered x-rays were collected in a 0.16 mm slit using a PIXcel3D detector. The reciprocal space map near the 103 peak was collected in a glancing exit geometry, using the PIXcel3D as a 14mm line detector to resolve many scattering angles simultaneously at each step in the scan. Finally, rocking curves were collected using a triple-axis detector for high resolution ω scans.

Piezo Force Microscopy:

PFM images were taken in an SPM XE-70 from Park Systems, by applying $0.7V_{RMS}$ between the grounded cantilever (ElectricCont-G from BudgetSensors) and the conductive substrate.

Polarization reversal was confirmed using the PFM tip to locally apply DC voltages between the grounded tip placed on the film surface, and the bottom conductive $SrTiO_3$:Nb substrate.

The details of Echem poling and PFM measurements are as follow:

1- To achieve large scale polarization on the catalytic surface, the samples were first poled a pristine $BaTiO_3$ film in a non-aqueous electrolyte (0.1 M LiClO4 in Polycarbonate) by applying ± 5V bias between sample and a Pt electrode. By exceeding the coercive field across the catalyst, we expect to achieve a polarization reversal across the whole surface.
2- To confirm the polarization reversal using electrochemical poling method, we investigated the phase of the pre-poled sample by PFM imaging confirming.
3- We then attempted to reverse the initial polarization by biasing a smaller area inside the first area by biasing the sample directly by PFM tip.
4- Finally, we attempted to reverse the domain directions written by PFM tip in previous step in a smaller area within the previously poled area. By doing this we reconfirmed the successful reversal of the domains by PFM tip as well as electrochemical poling.

Electrochemical Measurements:

All electrochemical experiments were performed using biologic potentiostat (VSP-300) in a gas-tight three electrode cell. Working electrodes were prepared from 5 mm × 5 mm samples by back-contacting Ti wires to Nb:$SrTiO_3$ using a small droplet of and silver paint (SPI supplies). After drying, we used non-conductive epoxy (Omegabond 101, Omega) to cover the back of the samples as well as the surface edges to prevent contact with the electrolyte. Cyclic voltammetry (CV) measurements were performed on pre-poled samples in a 0.1 M phosphate buffer electrolyte (pH=7.2) at voltages between -0.53 V and +0.4 V vs RHE. Before each experiment, the electrolyte was purged and saturated with N_2 before each experiment. We used mild pH conditions to avoid

any risk of film modifications at extreme pH. An Ag/Agcl (in 3M potassium Chloride (KCl), Pine Research) and graphite rode (Pine Research) were used as a reference electrode and counter electrode, respectively. The potentials reported herein are corrected by 85% automatic iR-compensation to the RHE scale. Tafel analysis was performed by running potentiostatic chronoamperometry (CA) measurements at different overpotentials for 5 minutes and averaging the current density (Fig. S3). Electrochemical impedance spectroscopy (EIS) measurements were performed at -0.48 V vs RHE between 50 mHz and 200 KHz. The charge transfer resistance was extracted by fitting a semi-circle to the Nyquist Plot based on Simplified Randles circuit using EC-Lab software.

Faradaic Efficiency Measurements:

The Faradaic efficiency of H_2 formation on $BaTiO_3$ surface was performed by running CA measurements for 60 minutes at -0.48 V vs RHE and quantifying the amount of generated H_2 in headspace and liquid phase. Prior to each experiment, we thoroughly cleaned all the electrochemical cell components with aqua regia to remove any metal impurities. Then the cell head space were purged with N_2 for 30 minutes. After the CA, 0.5mL aliquot was extracted from the headspace using a Luer-lock (Air-Tite) syringe and manually injected into a gas chromatograph (SRI 8610C MG3) equipped with a mol sieve column to separate permanent gasses and a thermal conductivity detector (TCD). Concentrations were quantified using similar manual injection of a reference gas standard (Research grade PRAXAIR calibration gas with 98.8 ppm of H_2). The amount of generated H_2 in the gas and liquid phase was calculated based on a 1.411×10^{-5} hydrogen solubility in water at 298K[4] and 35mL and 230 mL volumes for headspace and liquid phase, respectively. Average FE% values and standard deviations for experiments with at least 3 injections for each are presented Table S1.

$$\mathrm{n}H_2(\mathrm{g}) = \mathrm{C}(H_2) \times 35\mathrm{ml}/22400(\mathrm{mLmol}^{-1})$$

$$\mathrm{n}H_2(\mathrm{dissolved}) = \mathrm{C}(H_2) \times 1.411 \times 10^{-5} \times 230(\mathrm{mL}) \times 1(\mathrm{g/mL})/18(\mathrm{gmol}^{-1})$$

$$\mathrm{FE}(H_2) = \frac{\left(\mathrm{n}H_2(\mathrm{g}) + \mathrm{n}H_2(\mathrm{dissolved})\right) \times 2\ \frac{mol\ e-}{\mathrm{mol\ H_2}} \times 96485(\mathrm{Cmol}^{-1}))}{\int_0^t idt}$$

Xray Photoelectron Spectroscopy:

X-ray photoelectron spectroscopy (XPS) measurements and ultraviolet photoelectron spectroscopy (UPS) measurements were conducted using AXIS Supra XPS by Kratos Analytical using Al Kα radiation. For UPS measurements we used an unfiltered He I (21.22 eV) gas discharge lamp. For spectroscopic investigations, we used the same electrochemical poling method discussed previously, to expose the bare polarized surfaces responsible for the modulation of the electrocatalysis. Binding energies were calibrated based on adventitious C 1S at 284.8 eV. Background was subtracted using Tougaard[5] method and a Lorentzian/Gaussian Asymmetric Lineshape was used to fit core-levels. Details of binding energies of individual peaks and fitting parameters are listed in Table S2-3. Relative contribution of Ba (II) to Ba (I) core levels was calculated based on relative areas of fitted peaks at each grazing angle (Table S.4).

$$x = \frac{area\ of\ Ba(II)}{area\ of\ Ba(I)}$$

To compare the intensity of valance band DOS on poled up and poled down samples (Fig. S5), the spectra were calibrated based on Ba-5p pre-edge intensities.

DFT calculations:

To calculate the surface energies of different facets of $BaTiO_3$ we used the methodology previously described by Vanderbilt et.al based on cleavage energy of asymmetric and symmetric perovskite slabs.[6] The calculated surface energies are shown in Table S5, where we find that the TiO_2 terminated surface are the most energetically favorable, in good agreement with previously published results.[6] To accurately mimic the surface of a thick film, the first two-unit cells of $BaTiO_3$ in contact with the Pt electron reservoir were fixed at their bulk ferroelectric coordinates, while the top 4 layers were allowed to fully relax along with adsorbates until the residual forces on the atoms were smaller than a 0.01eV/Å threshold. We used a ~10Å thick vacuum on each side of the slabs in addition to dipole corrections to prevent spurious interactions between the opposite surfaces.

Free energy of adsorption for H* on polarized slabs were calculated using the following equation:

$$\Delta G_{H^*} = \Delta E + \Delta ZPE - T\Delta S + \Delta G(pH)$$

which includes contributions due to the binding energy (ΔE), differences in the zero-point energy (ΔZPE), change in the adsorption entropy (TΔS) and pH corrections.

i) ΔE is the calculated binding energy from DFT:

$$\Delta E = E(slab + H^*) - E(bare\ slab) - \frac{1}{2}E(H_2)$$

ii) Difference in zero-point energies (ZPE) was calculated based on the following equation:

$$\Delta(ZPE) = E_{zpe}^{H} - 1/2E_{zpe}^{H2}$$

iii) Considering negligible shifts in the phonon modes for H* adsorbed on the catalyst surface, we can express the entropic corrections as:

$$\Delta(S) = -1/2S_{H2}^{0}$$

where S^0_{H2} is the ideal gas entropy.

iv) The pH effects were calculated as:

$$\Delta G(pH) = -kT \times ln\,(10 \times pH)$$

Using ZPE and $T\Delta S$ values obtained from Ref [7] and a pH of ~7 (corresponding to our experimental conditions), we calculated the total correction to our binding energies as:

$$\Delta G_{H^*} = \Delta E + 0.14$$

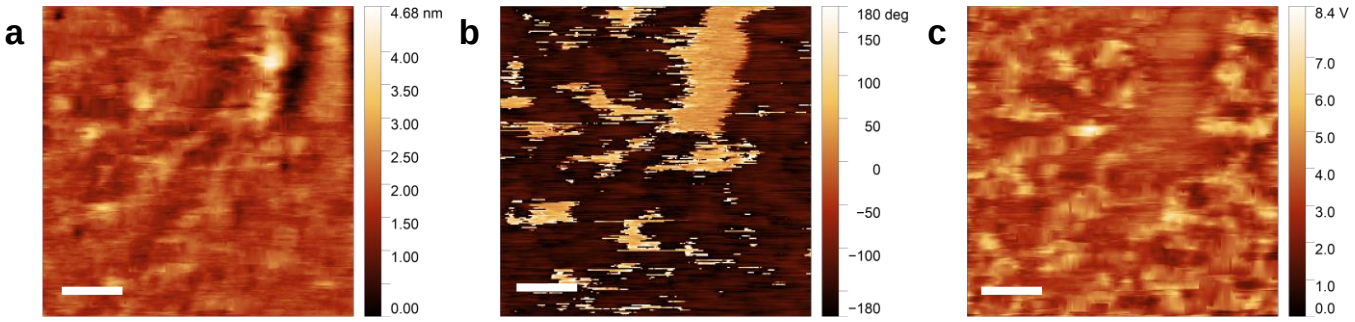

Figure S1. (a) topography, with a RMS roughness (R_q) of 428 pm. (b) phase and (c) amplitude PFM images of as grown sample, showing random orientation of domains. Scale bars are 100 nm.

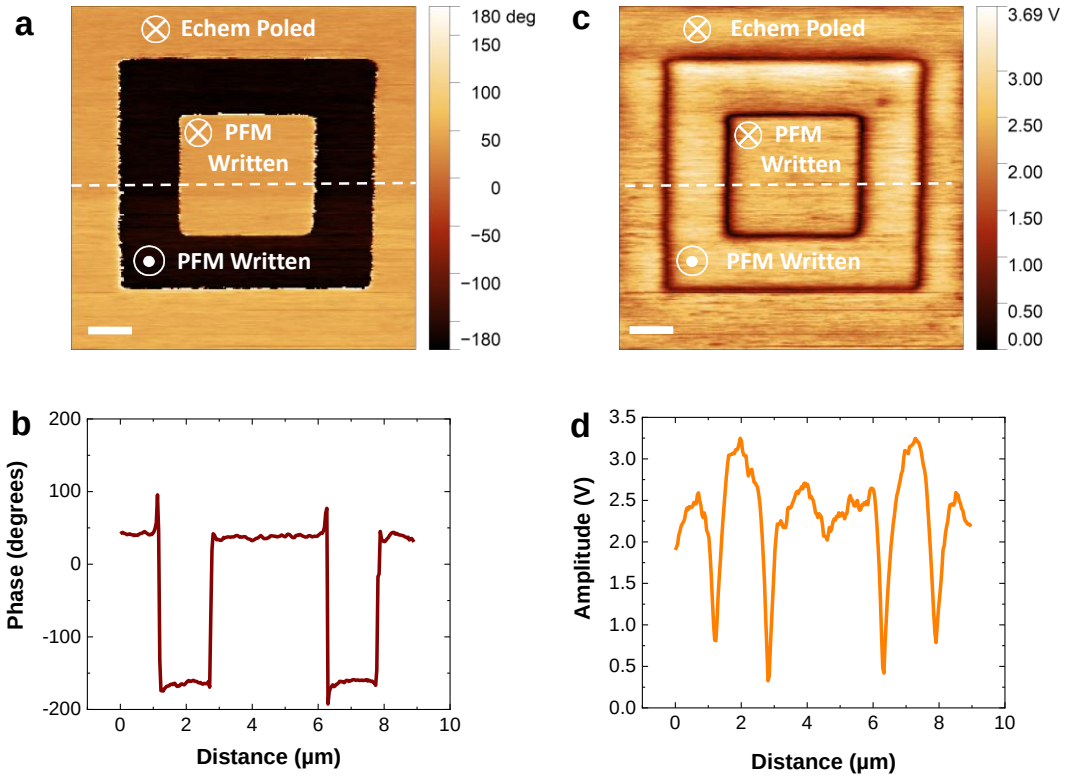

Figure S2. PFM image and corresponding line profile of (a-b) phase and (c-d) amplitude of the film first poled downward by the electrochemical method and then re-poled upward and downward using the grounded PFM tip. Scale bars are 1 μm.

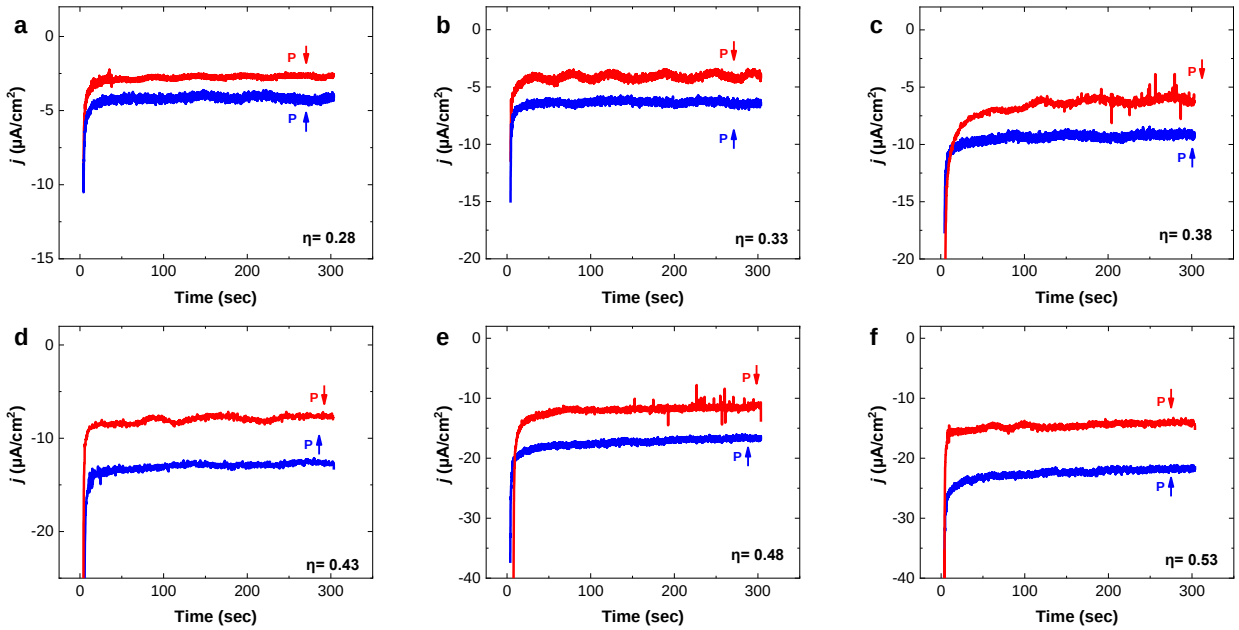

178

179 **Figure S3.** CA measurements at different overpotentials used to extract Tafel slopes.

180

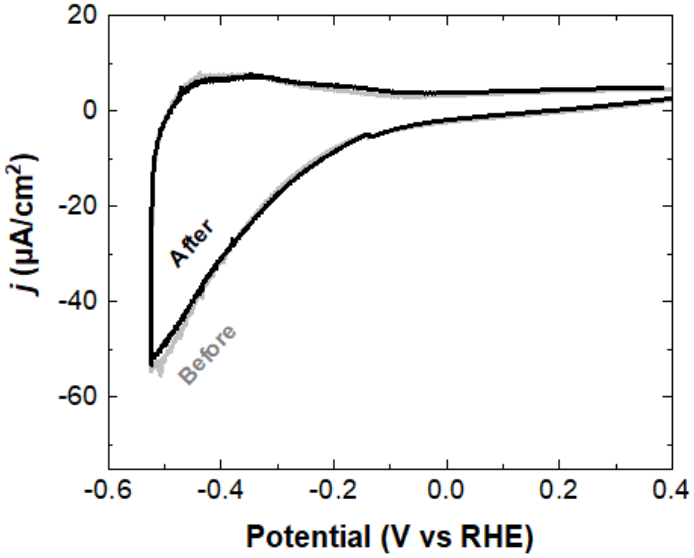

181

182 **Figure S4.** Cyclic voltammetry measurements before and after the consecutive CA measurements of Figure S3,
183 showing stability of the $BaTiO_3$ surface during HER reaction.

184

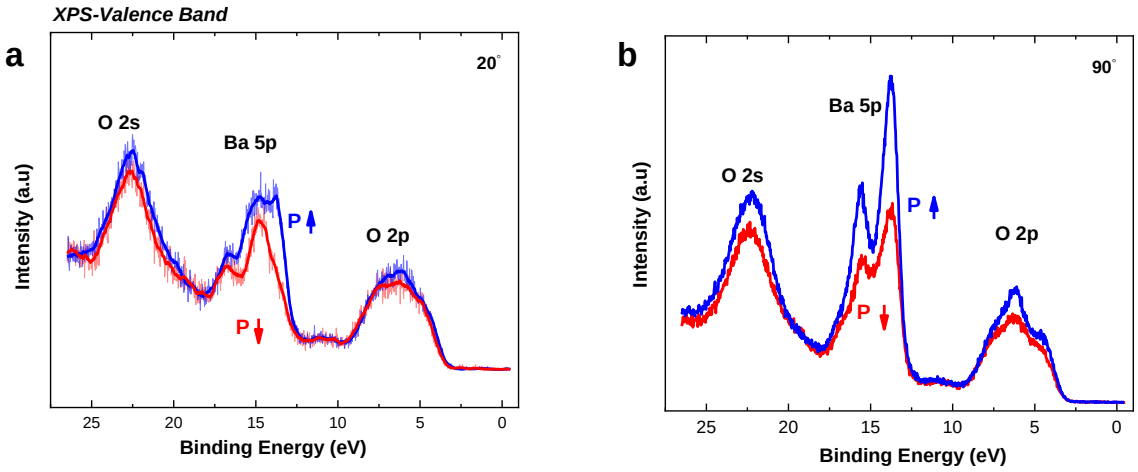

Figure S5. Valence-band XPS spectra at (a) 20° and (b) 90° takeoff angle on upward and downward films showing corresponding chemical states.

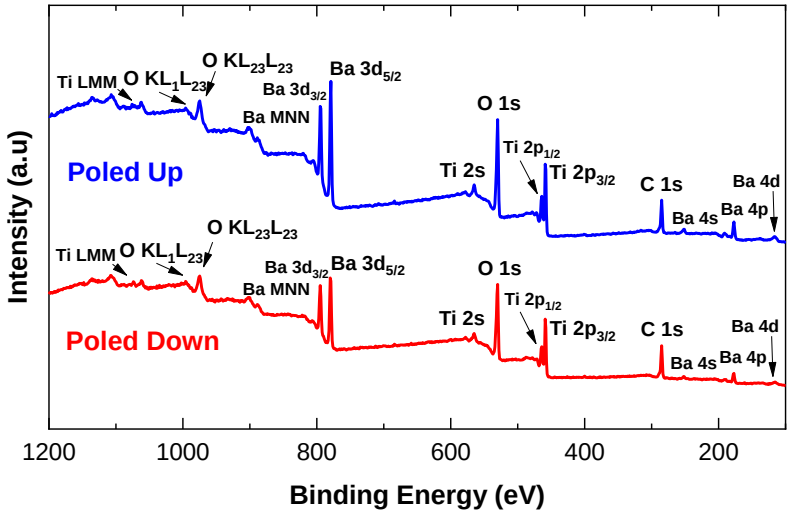

Figure S6. XPS survey spectrum of poled up and poled down samples.

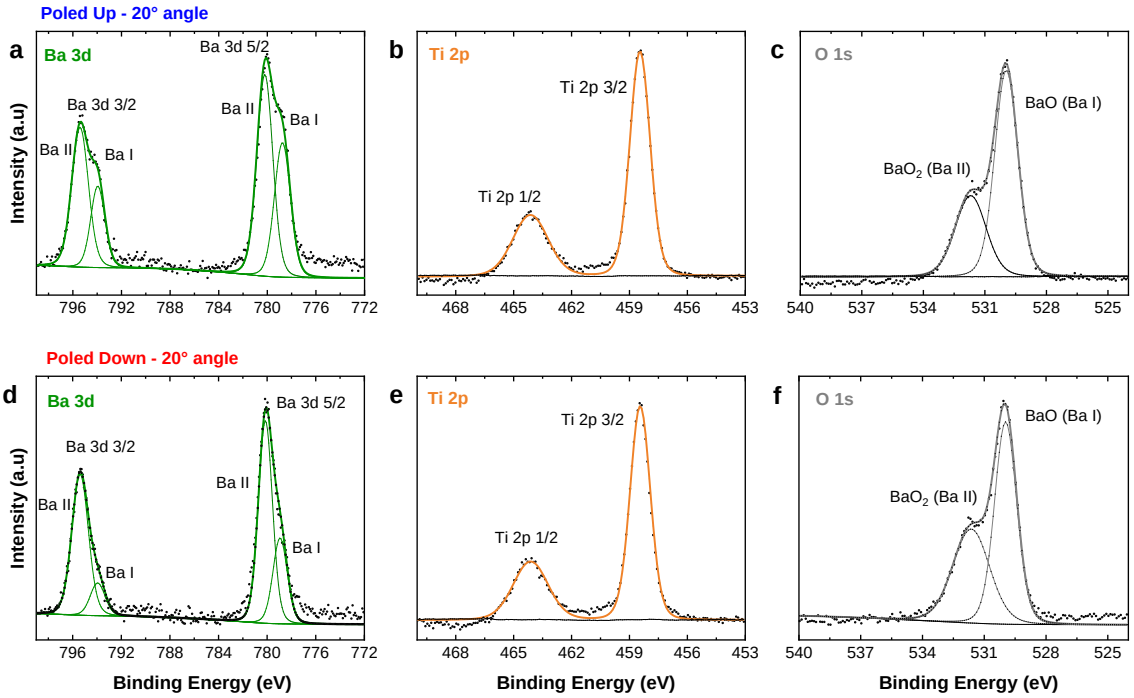

Figure S7. XPS core-level measurements at 20° takeoff angle of poled up (a-c) and poled down (d-f) samples.

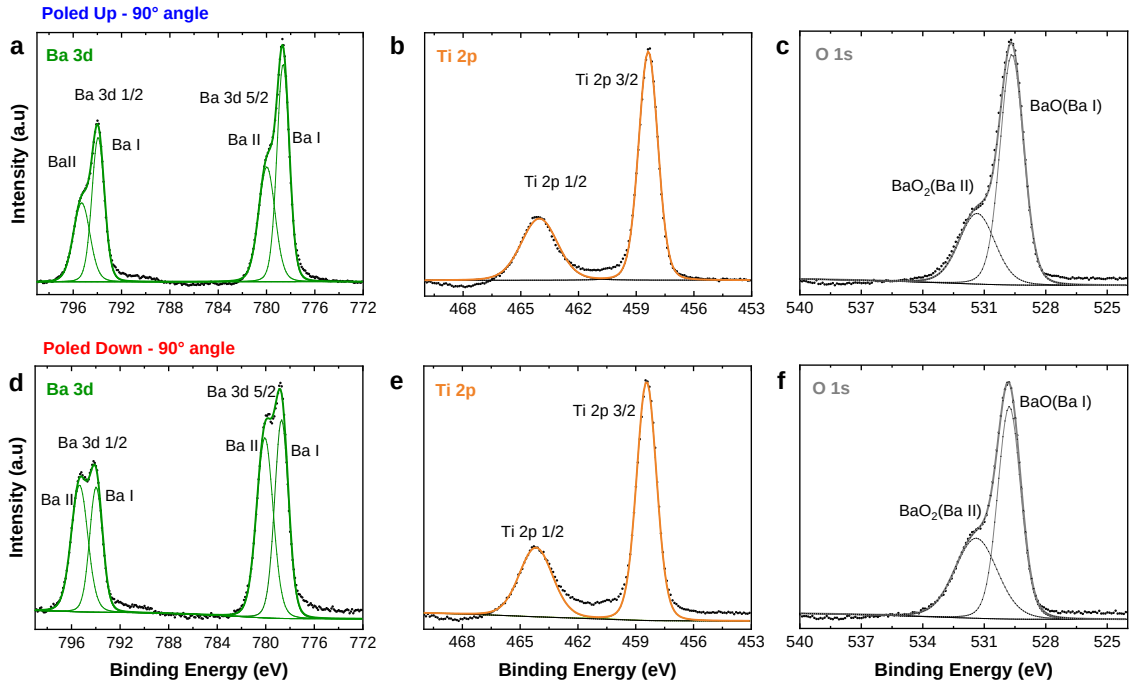

Figure S8. XPS core-level measurements at 90° takeoff angle of poled up (a-c) and poled down (d-f) samples.

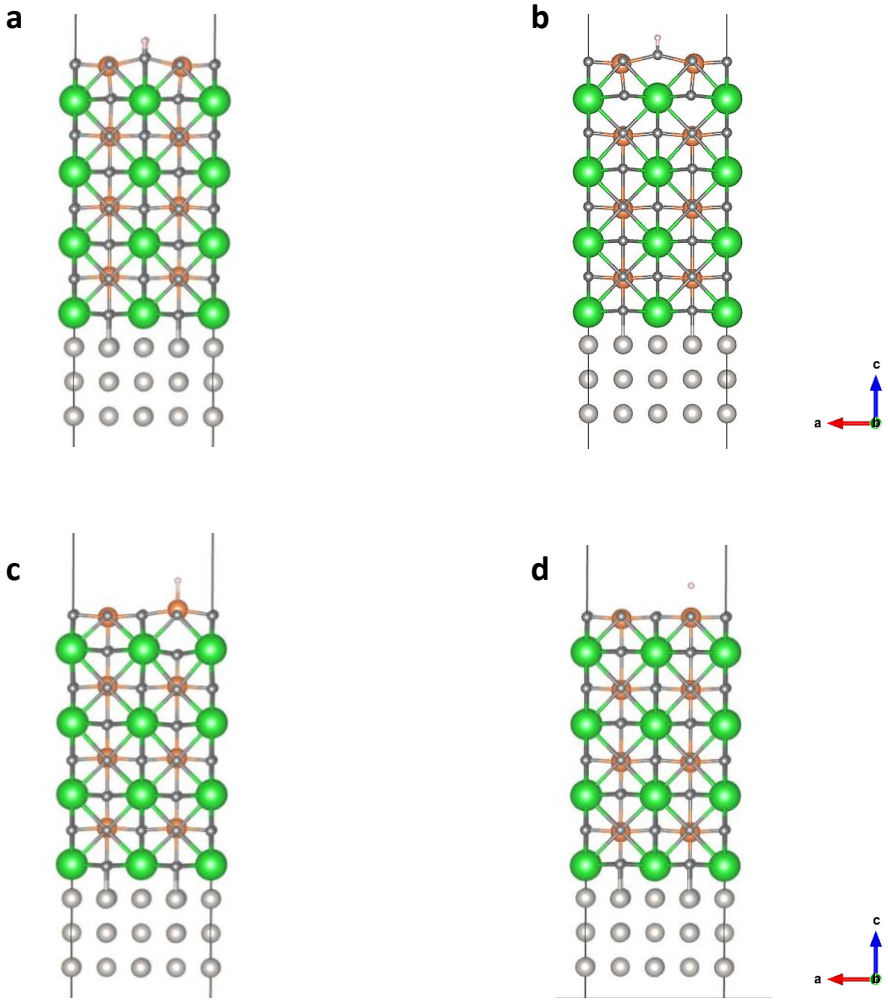

Figure S9. Snapshots of relaxed structures of (001) TiO_2-terminated slabs with H* atom adsorbed on O and Ti sites of **(a,c)** poled up and **(b,d)** poled down models. Ba, Ti, O, and H are shown with green, orange, gray, and white spheres, respectively.

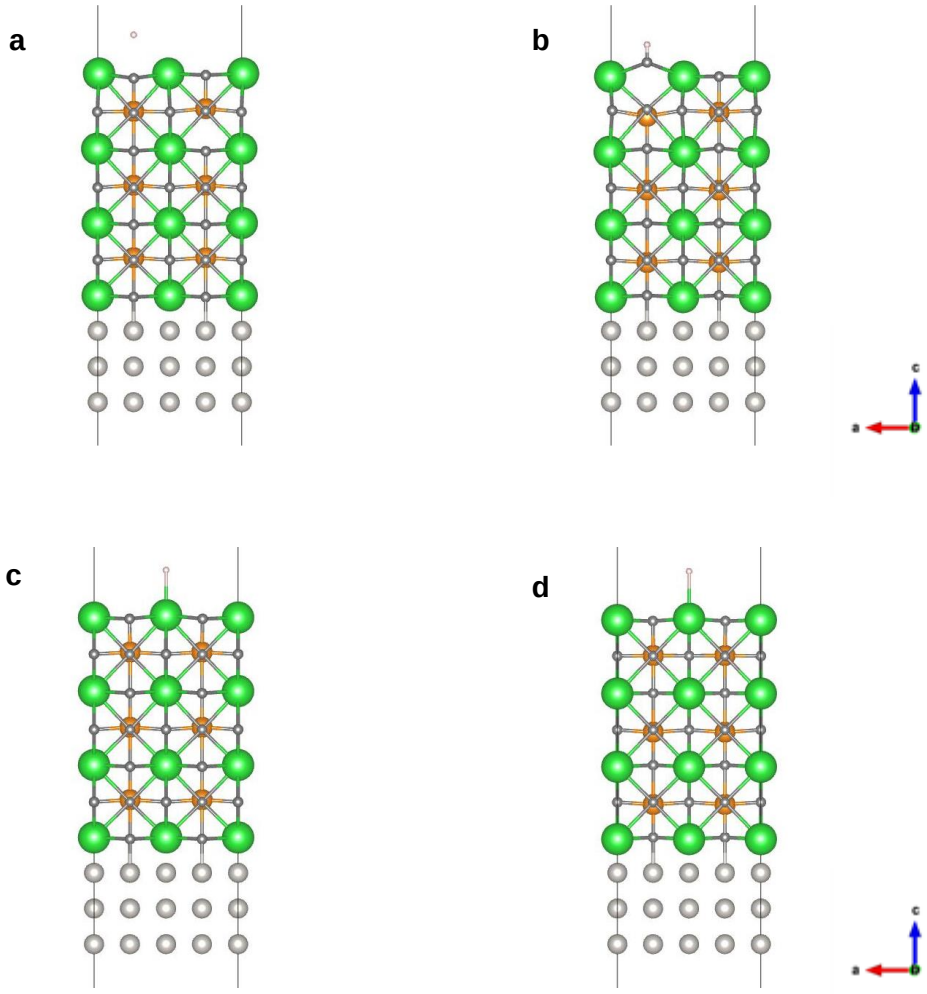

Figure S10. Snapshots of relaxed structures of (001) BaO-terminated slabs with H* atom adsorbed on O and Ba sites of **(a,c)** poled up and **(b,d)** poled down models. Ba, Ti, O, and H are shown with green, orange, gray, and white spheres, respectively.

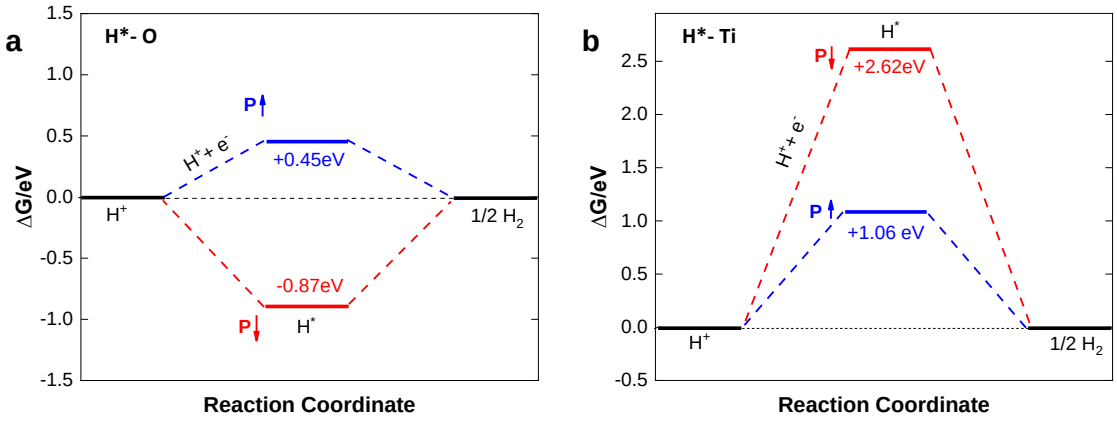

Figure S11. Reaction free energy for H_2 formation considering H* adsorption on **(a)** O site and **(b)** Ti site with upward (blue) and downward (red) polarization.

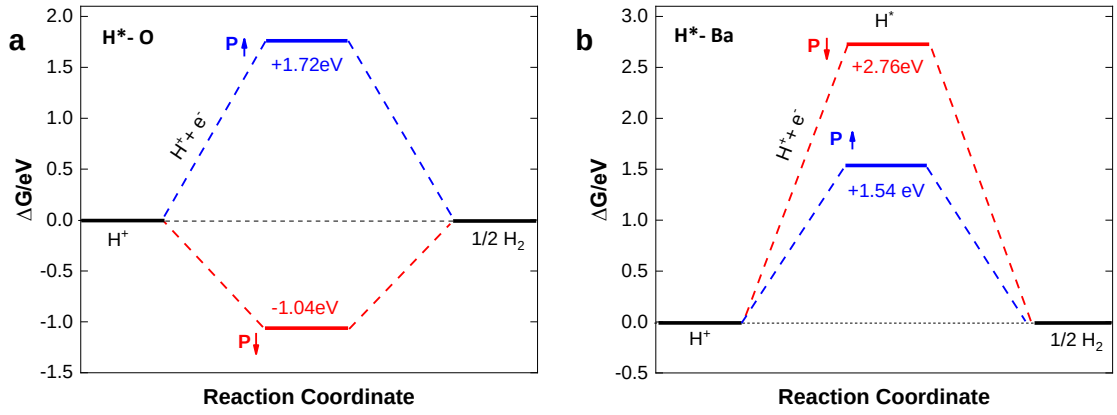

Figure S12. Reaction free energy for H_2 formation considering H* adsorption on **(a)** O site and **(b)** Ba site with upward (blue) and downward (red) polarization.

Table S1. Details of Faradaic efficiency measurements at η=0.48V.

Experiment#	Total Charge Passed (mC)	FE%	Std%
Experiment1	8.7	93.3	4.7
Experiment2	8.8	97.4	2.1
Experiment3	13.3	88.3	4.1
Avg FE%		93.0	3.6

Table S2. Position of core-levels in narrow scans for poled up and poled down samples at 90° takeoff angle.

90 degree	Poled Down		Poled Up	
Core-levels	**Binding Energy (eV)**	**FWHM**	**Binding Energy (eV)**	**FWHM**
Ba3d-5/2	778.7	1.34	778.6	1.20
Ba3d-3/2	780.1	1.60	780.0	1.60
Ba3d-5/2	794.0	1.26	793.9	1.22
Ba3d-3/2	795.3	1.61	795.3	1.62
Ti 2p-3/2	458.4	1.22	458.4	1.17
Ti 2p-1/2	464.2	2.04	464.0	2.22
O 1s	529.8	1.33	529.7	1.35
O 1s	531.4	2.43	531.4	2.05

Table S3. Position of core-levels in narrow scans for poled up and poled down samples at 20° takeoff angle.

20 degree	Poled Down		Poled Up	
Core-levels	**Binding Energy (eV)**	**FWHM**	**Binding Energy (eV)**	**FWHM**
Ba3d-5/2	778.90	1.39	778.80	1.55
Ba3d-3/2	780.10	1.36	780.20	1.55
Ba3d-5/2	793.90	1.43	794.00	1.37
Ba3d-3/2	795.40	1.61	795.40	1.62
Ti 2p-3/2	458.40	1.24	458.50	1.23
Ti 2p-1/2	464.10	2.13	464.10	2.17
O 1s	530.00	1.27	530.00	1.32
O 1s	531.60	2.10	531.70	1.77

Table S4. Relative contribution of Ba (II) to Ba (I) core levels.

Core-levels	Poled down 90°	Poled Up 90°	Poled down 20°	Poled up 20°
Ba 3d 3/2	1.29	0.72	4.84	2.02
Ba 3d 5/2	1.08	0.69	2.32	1.50

Table S5. Surface energies for different facets and terminations of tetragonal $BaTiO_3$.

Facet	**111**		**110**		**001**	
Termination	Ti	BaO_3	BaTiO	O	TiO_2	BaO
Surface Energy (eV/A^2)	0.138	0.155	0.177	0.151	0.051	0.061

Table S6. Band center position of polarized surfaces relative to Fermi level.

Band Center Position (eV)	**Ti-d**	**O-p**
Poled Up	0.61	-3.13
Poled Down	2.41	-1.28

References:

(1) Koster, G.; Kropman, B. L.; Rijnders, G. J. H. M.; Blank, D. H. A.; Rogalla, H. Quasi-Ideal Strontium Titanate Crystal Surfaces through Formation of Strontium Hydroxide. *Appl. Phys. Lett.* **1998**, *73* (20), 2920–2922. https://doi.org/10.1063/1.122630.

(2) Theis, C. D.; Schlom, D. G. Cheap and Stable Titanium Source for Use in Oxide Molecular Beam Epitaxy Systems. *J. Vac. Sci. Technol. A Vacuum, Surfaces, Film.* **1996**, *14* (4), 2677–2679. https://doi.org/10.1116/1.580185.

(3) Haeni, J. H.; Theis, C. D.; Schlom, D. G. RHEED Intensity Oscillations for the Stoichiometric Growth of SrTiO3 Thin Films by Reactive Molecular Beam Epitaxy. *J. Electroceramics* **2000**, *4* (2), 385–391. https://doi.org/10.1023/A:1009947517710.

(4) Rankin, D. W. H. CRC Handbook of Chemistry and Physics, 89th Edition, Edited by David R. Lide. *Crystallogr. Rev.* **2009**, *15* (3), 223–224. https://doi.org/10.1080/08893110902764125.

(5) Tougaard, S. Composition Depth Information from the Inelastic Background Signal in XPS. *Surf. Sci.* **1985**, *162* (1–3), 875–885. https://doi.org/10.1016/0039-6028(85)90992-6.

(6) Eglitis, R. I.; Vanderbilt, D. Ab Initio Calculations of BaTi O3 and PbTi O3 (001) and (011) Surface Structures. *Phys. Rev. B - Condens. Matter Mater. Phys.* **2007**, *76* (15), 1–9. https://doi.org/10.1103/PhysRevB.76.155439.

(7) Artrith, N.; Sailuam, W.; Limpijumnong, S.; Kolpak, A. M. Reduced Overpotentials for Electrocatalytic Water Splitting over Fe- and Ni-Modified BaTiO3. *Phys. Chem. Chem. Phys.* **2016**, *18* (42), 29561–29570. https://doi.org/10.1039/c6cp06031e.